Pasadena, CA for the use of their data. They would also like to acknowledge the useful comments by one anonymous reviewer.

REFERENCES

[1] J. C. Giampaolo, "An improved ocean surface emissivity wind speed correction," M.S. thesis, Pennsylvania State Univ., University Park, 1999.
[2] S. J. Keihm, V. Zlotnicki, and C. S. Ruf, "Topex Microwave Radiometer Performance Evaluation, 1992-1998," *IEEE Trans. Geosci. Remote Sensing*, no. 38, pp. 1379–1386, May 2000.
[3] E. P. McClain, W. G. Pichel, and C. C. Walton, "Comparative performance of AVHRR-based multichannel sea surface temperatures," *J. Geophys. Res.*, no. 90(C6), pp. 11 587–11 601, 1985.
[4] C. S. Ruf, S. J. Keihm, B. Subramanya, and M. A. Janssen, "TOPEX/Poseidon microwave radiometer performance and in-flight calibration," *J. Geophys. Res.*, no. 99, pp. 24 915–24 926, 1994.
[5] C. S. Ruf, "Detection of calibration drifts in spaceborne microwave radiometers using a vicarious cold reference," *IEEE Trans. Geosci. Remote Sensing*, no. 38, pp. 44–52, Jan. 2000.
[6] F. J. Wentz, "A model function for ocean microwave brightness temperatures," *J. Geophys. Res.*, no. 88, pp. 1892–1908, 1983.
[7] D. L. Witter and D. B. Chelton, "A GEOSAT altimeter wind speed algorithm and a model for altimeter wind speed algorithm development," *J. Geophys. Res.*, no. 96, pp. 8853–8860, 1991.
[8] T.T. Wilheit, "A model for the microwave emissivity of the ocean's surface as a function of wind speed," *IEEE Trans. Geosci. Remote Sensing*, vol. GE-17, pp. 244–249, 1979.
[9] M. H. Freilich and P. G. Challenor, "A model for the microwave emissivity of the ocean's surface as a function of wind speed," *J. Geophys. Res.*, vol. 99, pp. 25 501–25 062, 1994.

A Quantitative and Comparative Analysis of Linear and Nonlinear Spectral Mixture Models Using Radial Basis Function Neural Networks

Kerri J. Guilfoyle, Mark L. Althouse, *Member, IEEE*, and Chein-I Chang, *Senior Member, IEEE*

***Abstract*—A radial basis function neural network (RBFNN) is developed to examine two mixing models, linear and nonlinear spectral mixtures, which describe the spectra collected by both airborne and laboratory-based spectrometers. We examine the possibility that there may be naturally occurring situations where the typically used linear model may not provide the most accurate resultant spectral description. Under such a circumstance, a nonlinear model may better describe the mixing mechanism.**

***Index Terms*—Linear mixture, nonlinear mixture, radial basis function neural network (RBFNN).**

I. INTRODUCTION

Hyperspectral imaging spectrometers collect image cubes containing spectral data reflected from surface materials. Each pixel in an image cube contains the resultant mixed spectrum from reflected source radiation. This spectral data contain information about the component materials (endmembers) in the target region at the subpixel level. These imagers can be flown in either aircraft or on satellites and are used to study the endmember component structures of both terrestrial and planetary surfaces. The sensitivity ranges of these instruments typically lie between the visible and near-infrared ranges, for example, from 0.4 μm to 2.5 μm. The data collected by these spectrometers form an image cube that is typically on the order of 200 bands deep with complete images at each band. This paper investigates methods of interpreting such data cubes.

Historically, linear mixture models have been used to describe the resultant mixed spectra collected by hyperspectral imagers or laboratory-based spectrometers. However, it is also possible that a nonlinear mixture model may better describe the resultant mixture spectra for certain endmember distributions. It has been shown by Mustard and Pieters [1] that the use of a nonlinear mixture model that is based on Hapke's bidirectional spectroscopy theory [2], referred to as the intimate mixture model, improves abundance estimates in intimate mixtures of soils. In order to evaluate both of these mixing models, a tested set is developed in which both models can be easily applied and verified.

Linear mixture modeling is used to describe those situations in which the endmember components are distributed in block-like areas within the field-of-view (FOV) of the instrument. These situations may occur when the spectrometer FOV passes over discrete regions such as fields, lakes, rivers, and forests. In these cases, one would expect the resultant reflectance spectrum to be a linear combination of endmembers present in the region, for example, a river water component and perhaps a soil component (for the river bank). The linear model assumes that source radiation is singly reflected from the endmember substances and then collected by the imaging spectrometer.

Nonlinear mixtures occur in situations where endmember components are randomly distributed throughout the FOV of the instrument. Such situations may occur, for example, when viewing striated soils, in areas where multiple rock types are all visible on the region's surface, or in identifying trees in a forest (assuming reflectance spectra differences exist). In these cases, the resultant mixture reflectance spectrum may best be described by assuming that source radiation is multiply scattered by the randomly distributed endmembers before being collected by the imaging spectrometer. Experiments are conducted in such a manner that linear and nonlinear mixtures have been created with colored sand according to the above descriptions, and the resultant mixed spectra are analyzed. The results show that the nonlinear model does match the randomly distributed mixture spectra, while the linear model better matches the discrete region mixture [3].

In order to estimate the abundance of given endmember components using both models, a radial basis function neural network (RBFNN) is developed. It is based on a similar network designed by Leung and Lo [4] for the estimation of the angles of arrival of signals at an antenna. The Leung and Lo network was modified for abundance estimation by creating a test set using the known endmember data and comparing true mixture data with the test data.

II. SPECTRAL MIXTURE MODELS

In many current hyperspectral imagery applications, the spectrum of an image pixel is typically described by a linear mixture which can be modeled as a linear combination of image endmember components weighted by their abundance values as follows:

$$\mathbf{r} = \mathbf{M}\boldsymbol{\alpha} + \mathbf{n} \tag{1}$$

where

- $\mathbf{r}$ resultant spectrum of an image pixel vector with $\boldsymbol{\alpha}$ corresponding to the abundance column vector;
- $\mathbf{M}$ endmember spectra matrix;
- $\mathbf{n}$ noise vector.

Manuscript received April 11, 2000; revised September 7, 2000.

The authors are with the Remote Sensing and Image Processing Laboratory, Department of Computer Science and Electrical Engineering, University of Maryland, Baltimore County, Baltimore, MD 21250 USA (e-mail: cchang@umbc.edu).

Publisher Item Identifier S 0196-2892(01)05483-3.

A nonlinear model considered in this paper is based on the radiative transfer theory presented by Chandrasekhar in 1960 [4]. Chandrasekhar's theory was modified for bidirectional reflectance by Hapke [2]. In this description, the resultant mixed spectrum is created by both a single scattered component and a multiple scattered component. This model incorporates the surface and reflecting properties of the component substances as well as the angles of illumination and detection in the description of the total reflected radiation spectrum. Hapke [2] developed an approximate solution to the radiative transfer function for a specific case of light scattering from particulate surfaces. This approximate solution was then modified for remote sensing applications by Mustard [1] and Johnson [5]. Hapke's solution for the resultant spectral radiance of a surface, $I(\mu, \mu_0, g)$ is given by

$$I(\mu, \mu_0, g) = I_0 \frac{\omega}{4\pi} \frac{\mu_0}{\mu_0 + \mu} \times \left[P(g)(B(g)+1) + H(\mu_0)H(\mu) - 1\right]. \tag{2}$$

where

I_0	radiated source intensity;
ω	single scattering albedo;
μ	$\cos\theta_e$;
θ_e	angle of emergence;
μ_0	$\cos\theta_i$;
θ_i	angle of incidence;
g	phase angle;
B	backscatter function;
P	average single particle phase function;
B	backscatter function.

In the data experiments that follow, approximations to $B(g) = 0$ (i.e., negligible for phase angles of greater than 15°) and $P(30^\circ) = 1$ have been used. These approximations have been used with success in previous experiments by Mustard and Pieters [1] and Johnson *et al.* [5] and will be explained in greater detail later in this section. Hapke's approximation to Chandrasekhar's function is given by

$$H(\mu) = \frac{1 + 2\mu}{1 + 2\mu(1-\omega)^{1/2}} \tag{3}$$

and has been used in this analysis instead of the exact integral to save computational time. This approximation holds as long as the endmembers are not high albedo substances. In all of the following experiments, the approximation to $H(\mu)$ should not greatly affect the abundance estimate. According to the work performed by Johnson *et al.* [5], the albedo of a mixture is a linear combination of the single-scattering albedos of its endmember constituents. Thus, if we can convert all of the pixels in an image to albedo, the popular linear unmixing methods for estimating abundance should provide more accurate results. With the above assumptions $(B(g) = 0, P(30^\circ) = 1)$ (2) leads to a final equation for the reflectance of

$$R = \frac{I(\mu, \mu_0, g)}{I_0 R_L} = \frac{\omega}{4(\mu_0 + \mu)} \left[H(\mu_0)H(\mu)\right]$$
$$\text{where } R_L = \frac{\mu_0}{\pi}. \tag{4}$$

III. Radial Basis Function Neural Networks

The radial basis function neural network (RBFNN) developed by Leung and Lo [6] for direction of arrival (DOA) mapping will be used to examine the mixing models described in Section II. In Leung and Lo's RBFNN, the network determined an estimated θ (direction of arrival) by comparing the received signal with a simulated "ideal" array signal. Since we are interested in the estimation of the abundance value(s) of a given endmember or set of endmembers, we will build an RBFNN that acts as an interpolative associative memory. In this case, the network will interpolate abundance values to best approximate the training data set created from known endmember spectra. How well these estimated abundance values match the true abundance values is determined by two network parameters: the number of hidden nodes and the node radius of activation function σ. If a mixing mechanism is described by a model specified by $\mathbf{y} = \mathbf{F}(\boldsymbol{\alpha}, \mathbf{M})$ where $\boldsymbol{\alpha}$ is the true abundance vector, and $\mathbf{M}$ is an endmember spectra matrix made up of known endmembers defined by (4), an RBFNN finds an inverse mapping $\mathbf{F}^{-1}$ to interpolate $\boldsymbol{\alpha} = \mathbf{F}^{-1}(\mathbf{y}(\alpha, \mathbf{M}))$. Of particular interest is the interpolating function $\mathbf{F}(\mathbf{y}) = \sum_i w_I \Phi_i(\|\mathbf{y} - \mathbf{y}_i\|)$, which will be a linear combination of nonlinear functions where Φ_i is radial basis function kernel, $\mathbf{y}_i$ is the center of Φ_i, and w_i is its corresponding weight. While the radial basis function kernel can be any radially symmetric function, the implementation in our experiments used a Gaussian kernel given by $\Phi_i(\mathbf{y}_i) = \exp\left(-(\mathbf{y} - \mathbf{y}_i)^2 / 2\sigma_i^2\right)$ where the value of σ_i^2 determines the radius of the activation function Φ_i of hidden node i. The resulting mixing model can be described by $\mathbf{F} = \mathbf{w}\boldsymbol{\Phi}$ where $\mathbf{w}$ is a weight vector formed by the w_is, and $\boldsymbol{\Phi}$ is a vector function made up of the $\boldsymbol{\Phi}_i$s. The estimated weight vector can be therefore obtained by $\mathbf{w} = \mathbf{F}\boldsymbol{\Phi}^{\#}$ where $\boldsymbol{\Phi}^{\#}$ is the pseudo-inverse of $\boldsymbol{\Phi}$ given by $\boldsymbol{\Phi}^{\#} = (\boldsymbol{\Phi}^{\mathrm{T}}\boldsymbol{\Phi})^{-1}\boldsymbol{\Phi}^{\mathrm{T}}$. Once these weights are calculated, the network is trained to interpolate an estimated abundance values based on that training set. Since there is no adaptive "learning" necessary, the network is now ready for input data vector processing. It should be noted that the ability of the network to estimate endmember abundance value is generally dependent on the number of hidden nodes, training parameters used in the hidden nodes, and radius of node activation. Since this paper is devoted to investigation of mixing mechanisms, finding optimal network parameters for the RBFNN is beyond its scope.

For the network developed here, the training data set is created by known endmembers used to compute binary mixtures for both linear and nonlinear models at a series of abundance values between 0 and 1. The number of training vectors N (and hence, the number of hidden nodes) is determined by the abundance step size δ with $N = 1/\delta$. Thus, the training data for the binary mixtures was created using the binary mixture equation given by $\mathbf{y}_i = \alpha_i \mathbf{E}_1 + (1 - \alpha_i)\mathbf{E}_2$ where $\mathbf{y}_i$ is the i-th training vector, $\mathbf{E}_i$ is the i-th endmember, and $0 \leq \alpha_i \leq 1$ is the true abundance value of $\mathbf{E}_1$ contained in $\mathbf{y}_i$. It should be noted that the abundance values were chosen randomly between 0 and 1, and the number of hidden nodes is equal to the number of random values selected.

The data analysis conducted in this paper studies the abundance estimation results obtained by two networks, one based on the linear model, and one based on the nonlinear model. For the linear case, the training data were created using (1), with the endmember spectra described by reflectance values. For the nonlinear case, the training set was created by first converting the endmember spectra to albedos using the modified Hapke method, then calculating the mixture (assuming that the albedo of a mixture is a linear combination of endmember albedos) and finally converting each resultant training vector back to reflectance values by using a reverse look-up table. This method has some computational advantages and may also have some accumulating error disadvantages as well. By converting the training vectors back to reflectance values, the RBFNN can compare the input data to the nonlinearly mixed training data directly without having to perform the time consuming task of converting each input data vector to albedos for comparison. The conversion of the input data vectors to albedos using the look-up table becomes time consuming for the AVIRIS data, where the input images contain 614×512 (314 368) pixels. However, any errors (either caused by random noise or deficiencies inherent in the nonlinear model) may be amplified during converting the training vectors back

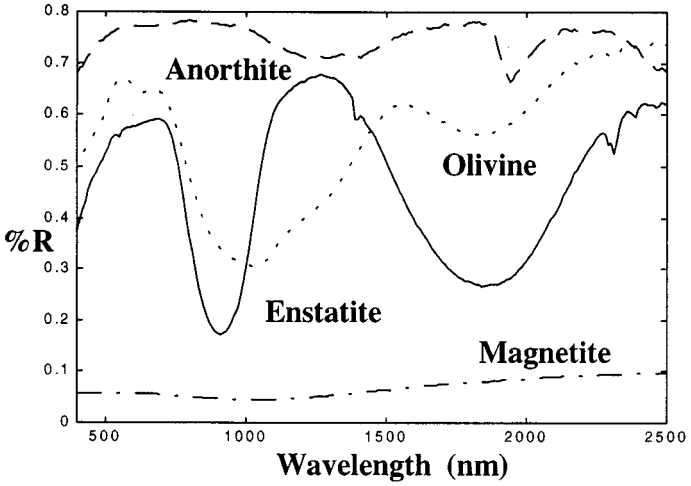

Fig. 1. Laboratory reflectance spectra.

to reflectance. This creates the possibility for an error increase in the abundance estimation. In the data analysis that follows, the results of both methods will be discussed.

The capability of the proposed RBFNN to accurately estimate the true abundance value of an endmember in input spectrum is dependent on two learning parameters: the number of hidden nodes (N) and the node radius of activation σ. In order to verify the use of this RBFNN as an abundance estimator, the networks needed to be optimized for N and σ. This was done by examining the effects of varying both N and σ in each of linear and nonlinear networks, and comparing the estimated abundance values with the known abundance values provided in Mustard's data. The results of these comparisons will be discussed in the following section.

IV. Computer Simulations

The objective of computer simulations is to use laboratory data at our disposal to design various scenarios to verify the utility of the RBFNN in solving nonlinear mixing problems. Furthermore, nonlinear mixing results will be compared with linear mixing results to show that the performance can be improved by nonlinear mixture modeling. Two types of data will be used in these simulations. Data sets provided by Dr. J. Mustard, Brown University, Providence, RI, will be used to validate the RBFNN method by comparing results against those obtained by Mustard [1]. Another data set from an airborne visible/infrared imaging spectrometer (AVIRIS) data cube collected over Cuprite, NV will be used to test the effectiveness of the RBFNN method in a closer-to-real world application. Mustard's data consist of 14 data sets collected using the RELAB spectrometer (a high resolution, bidirectional spectrometer at Brown University). These data included spectra from individual endmembers (olivine, anorthite, enstatite, and magnetite), which are shown in Fig. 1. The binary mixture data were the spectra of true mixtures with known abundance values for each endmember.

The first experiments involved the application of the RBFNNs to binary mixtures of olivine/enstatite, olivine/magnetite, and olivine/anorthite. The binary mixture data included mixtures with different ratios of both substances for each of the three binary mixture data sets. These experiments consisted of two sections: a comparison of the results of the RBFNN with both the linear and nonlinear models and a series of nonlinear RBFNN tests to determine optimum network operation and examine the effects of varying N and σ. In both cases, the results were compared with the results published in [1]. In all of the following experiments, the criterion of mean-squared error (MSE) was used for

TABLE I
Results of Binary Mixture Analysis for Olivine/Enstatite Samples

Actual Mass Fractions		*Non-Linear Radial Basis Function Computed Mass Fractions sigma=2.5*			*Linear Radial Basis Function Computed Mass Fractions sigma=0.9*		
Olivin	**Enstati**	**Olivine**	**Enstatite**	**MSE***	**Olivine**	**Enstatite**	**MSE***
0.90	0.10	0.8818	0.1149	0.0276	0.8635	0.1107	1.010
0.75	0.25	0.7006	0.2953	0.225	0.6683	0.2806	3.802
0.50	0.50	0.4431	0.5513	0.294	0.4133	0.5151	3.868
0.25	0.75	0.2303	0.7619	0.0264	0.2109	0.7051	1.775
0.10	0.90	0.1213	0.8755	0.0528	0.1174	0.8504	1.374

*mean-square error ($\times 10^{-3}$)

TABLE II
A Comparison of the RBFNL Results With Results Obtained by Nonlinear Least Squares Method (LSM)

Actual Mass Fractions		*Non-Linear Radial Basis Function Computed Mass Fractions sigma = 10*			*Mustard Computed Mass Fractions*		
Olivin	**Magneti**	**Olivine**	**Magnetite**	**MSE***	**Olivin**	**Magnetit**	**MSE**
0.95	0.05	0.9461	0.0313	0.0183	0.981	-0.028	0.352
0.90	0.10	0.8999	0.7503	0.0312	0.922	0.012	0.411
0.75	0.25	0.7651	0.1998	0.137	0.798	0.064	1.85
0.50	0.50	0.5768	0.4072	0.726	0.556	0.316	1.85
0.25	0.75	0.3007	0.6930	0.291	0.278	0.624	0.833

*mean-square error ($\times 10^{-3}$)

comparisons between the linear and nonlinear approaches and between Mustard's results and those presented here.

As mentioned previously, two network parameters, the number of training vectors (N), and the radius of hidden node activation σ determined an optimal interpolation. For an initial comparison of the linear versus nonlinear, the network was set up as follows: abundance step size $1/N = \delta = 0.01$ and $\sigma = 1$. These parameters were used for both the linear model and the nonlinear model. While the same parameters were used for each of these initial tests, both models require different σ values for optimum performance in the MSE sense. Following the initial comparison, each network was optimized for the input data set. The abundance step-size δ was held constant at 0.005 for each network, which is equal to 200 hidden nodes.

Table I shows a sample comparison between the nonlinear and linear RBFNNs, referred to as RBF-L and RBF-NL networks, respectively, for the olivine/enstatite binary mixture. Table II shows a comparison of the results produced by the RBF-NL network with the results presented in [1] for olivine/magnetite. Although limited space precludes tabulating all the results, in most cases, the nonlinear method generated a substantially better mass fraction estimate than did the linear method. These results indicate that the RBFNN computes mass fraction values that are similar in error values to the nonlinear least squares method employed by Mustard in [1]. In fact, the systematic errors (errors indicating a bias in the model) noted in [1] were reflected in the RBF-NL results, but not in the RBF-L results. This indicates that the error inherent in the RBFNN is less than the systematic errors in the nonlinear model itself.

Up to now, computer simulations were used to demonstrate the effectiveness of RBFNNs in nonlinear spectral mixture analysis. Next we will use a data set simulated from real AVIRIS spectra to further indicate possible advantages of using a nonlinear model over a linear model in certain detection situations. In order to conduct a quantitative analysis, absolute ground truth is required. The simulated image was created by extracting "target" and "background" pixels from an AVIRIS image and creating new images using both linear and nonlinear binary mixing methods. The "target" and "background" pixels were selected by choosing two pixels that had obviously different spectral properties

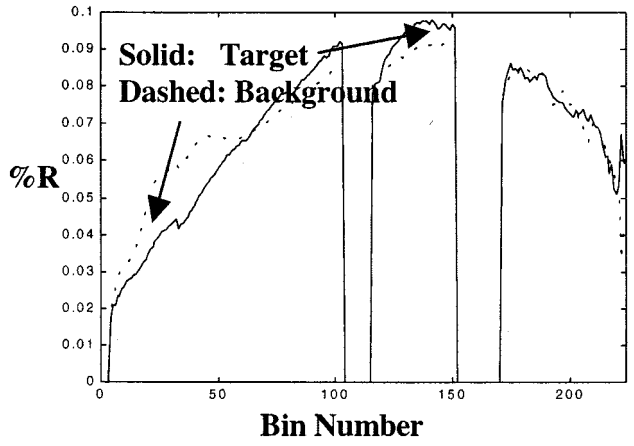

Fig. 2. Background and target signatures used in simulated AVIRIS images.

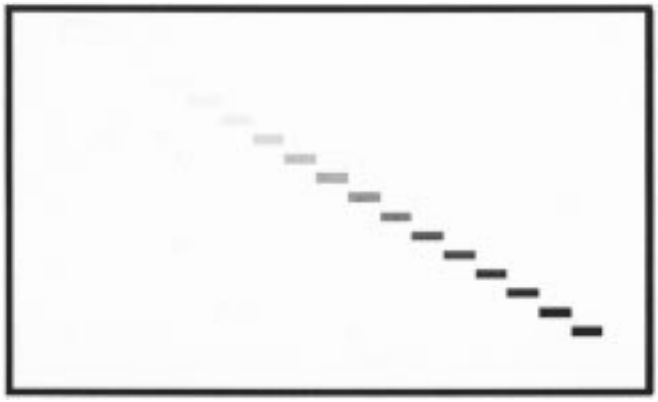

Fig. 3. Sample simulated AVIRIS images.

(see Fig. 2). The two simulated images (one linear and one nonlinear) consisted of a background image with 17 targets placed down the diagonal with varying abundance values. For these two images, the targets were generated by appropriately mixing the background and target spectra in the desired abundance amounts (see Fig. 3). In both data sets, each target was a 2×2 pixel area, while each data set had a total image size of 40×40 pixels. These two AVIRIS image cubes were then used in a series of experiments to determine the effectiveness of using a nonlinear spectral mixing model versus a linear spectral mixing model in identifying targets.

There are four possible experiments that can be performed using the above two images by the two RBFNNs, RBF-L, and RBF-NL previously described. These data sets can be used to test the effectiveness of the RBFNNs in detecting targets within an image as well as investigate the consequences of using a wrong model for detection. The four combinations are: 1) linearly mixed data using the linear detection methods; 2) nonlinearly mixed data using the linear detection method; 3) linearly mixed data using the nonlinear detection method; and 4) nonlinearly mixed data using the nonlinear detection method. In each of these experiments, the RBFNN was applied using a known target spectrum, and an estimated background spectrum. The background was estimated by averaging 100 spectra chosen randomly from each image. There is a definite relationship between the abundance estimation success of the RBFNN and the accuracy of the estimated background spectra. It is logical to believe that the accuracy of the abundance values would deteriorate if the estimated background vector does not closely match the true "background" or nontarget endmembers in each pixel. Detection curves were created using the results of these experiments to compare the results of all four experiments shown in Figs. 4 and 5. Fig. 5 was created by subtracting the estimated abundance values from the true abundance values and plotting the residuals. These curves show that the results of these experiments were very similar through most of the abundance values. Table III shows the actual abundance estimates for all four experiments. It is clear from these curves and Table III that no visible differences appear between the detection methods until the abundance values drop below 0.1 (see Fig. 5). The linear detection method for both linearly and nonlinearly mixed data performed poorly below abundance values of 0.05%. The nonlinear detection method worked

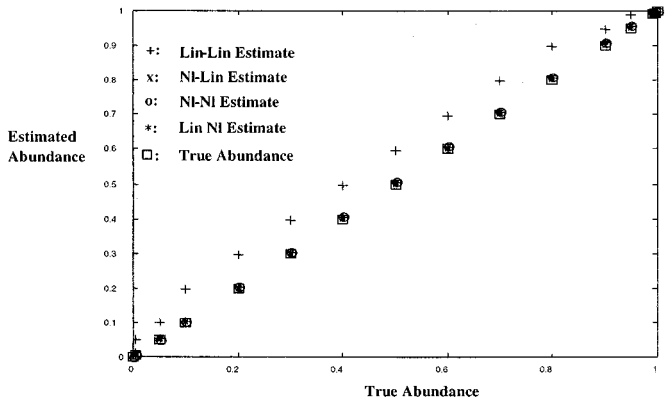

Fig. 4. True abundance versus estimated abundance for various methods.

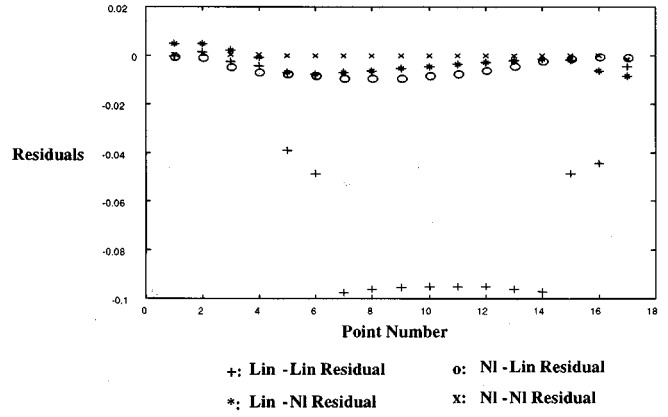

Fig. 5. Residuals between true abundance and estimated abundance for various methods.

TABLE III
COMPARATIVE STUDY AMONG FOUR DETECTION METHODS

Linear – Linear Abundance Estimates	Linear – Non-linear Abundance Estimates	Non-linear – Linear Abundance Estimates	Non-linear – Non-linear Abundance Estimates	True Abundance Values
0.9946	1.0000	0.9999	0.9991	0.9995
0.9943	0.9976	0.9999	0.9983	0.9990
0.9930	0.9975	0.9997	0.9948	0.9950
0.9908	0.9942	0.9966	0.9898	0.9900
0.9572	0.9892	0.9575	0.9500	0.9500
0.9077	0.9485	0.9083	0.9000	0.9000
0.8072	0.8977	0.8091	0.8000	0.8000
0.7064	0.7962	0.7093	0.7000	0.7000
0.6055	0.6953	0.6092	0.6000	0.6000
0.5046	0.5949	0.5082	0.5000	0.5000
0.4037	0.4949	0.4075	0.4000	0.4000
0.3029	0.3952	0.3061	0.2999	0.3000
0.2021	0.2960	0.2042	0.2000	0.2000
0.1015	0.1972	0.1022	0.1000	0.1000
0.0517	0.0985	0.0512	0.0500	0.0500
0.0115	0.0493	0.0053	0.0050	0.0050
0.0089	0.0053	0.0012	0.0018	0.0005

well on both linearly and nonlinearly mixed data, however, down to 0.005% abundance. More target areas were detected by the nonlinear detection method for both linearly and nonlinearly mixed data.

V. Conclusion

The experiments conducted in this paper have shown that the RBFNN was a useful tool for performing abundance estimation and target detection in both laboratory spectrometer and hyperspectral imagery data. The RBFNN used in this analysis was easily adaptable to either the nonlinear or linear mixture model. The resulting abundance estimates in most cases were at least as accurate as those calculated by the nonlinear LSM employed by Mustard [1]. The experiments performed in this analysis also indicated areas where nonlinear detection methods for targets in hyperspectral imagery might prove more effective than linear methods. While a linear detection method might work adequately for many scenarios, there are possibly naturally occurring scenarios where a nonlinear detection method might perform better. These scenarios may be targets of small abundance (less than 0.1%), situations where small target areas were dispersed throughout the image area or situations where accuracy is required. As a result of this analysis, some areas that need further study have been identified. All of the above hyperspectral experiments were performed in a relatively noise-free environment. Further experiments are needed to determine a detection curve for the nonlinear method versus SNR. The hyperspectral experiments presented in this paper only consisted of binary mixtures, which were intended to show the usefulness of the nonlinear detection method. Additional experiments using both ternary or quaternary mixtures, as well as real AVIRIS images with known abundance values, should be performed to arrive at more conclusive results.

Acknowledgment

The authors would like to thank Dr. J. Mustard, Brown University, Providence, RI, for providing the initial data sets used as a base for the experiments conducted in this paper and also for providing technical support during the early stages of the experiments.

References

[1] J. F. Mustard and C. M. Pieters, "Photometric phase functions of common geologic minerals and applications to quantitative analysis of mineral mixture reflectance spectra," *J. Geophys. Res.*, vol. 94, no. B10, pp. 13 619–13 634, Oct. 1989.

[2] B. Hapke, "Bidirectional reflectance spectroscopy, 1, theory," *J. Geophys. Res.*, vol. 86, pp. 3039–3054, 1981.

[3] K. Guilfoyle, M. L. G. Althouse, and C.-I. Chang, "Spectral mixture modeling for spatially distinct and randomly distributed regions," in *Proc. 1999 Int. Symp. Spectral Sensing Research*, Oct.–Nov. 31–3, 1999.

[4] S. Chandasekhar, *Radiative Transfer*. New York: Dover, 1960.

[5] P. E. Johnson, M. O. Smith, and J. B. Adams, "Simple algorithms for remote determination of mineral abundances and particle sizes from reflectance spectra," *J. Geophys. Res.*, vol. 97, pp. 2649–2657, Feb. 1992.

[6] H. Leung and T. Lo, "Array processing using radial basis function neural network," in *Advances in Spectrum Analysis and Array Processing*, S. Haykin, Ed. Englewood Cliffs, NJ: Prentice-Hall, 1995, vol. III, ch. 10, pp. 510–539.